PNAS RESEARCH ARTICLE | BIOPHYSICS AND COMPUTATIONAL BIOLOGY

The optimal docking strength for reversibly tethered kinases

Mateusz Dyla[a,1,2], Nicolás S. González Foutel[a,1], Daniel E. Otzen[a,b], and Magnus Kjaergaard[a,b,c,d,3]

Edited by Natalie Ahn, University of Colorado Boulder, Boulder, CO; received February 20, 2022; accepted May 10, 2022

Many kinases use reversible docking interactions to augment the specificity of their catalytic domains. Such docking interactions are often structurally independent of the catalytic domain, which allow for a flexible combination of modules in evolution and in bioengineering. The affinity of docking interactions spans several orders of magnitude. This led us to ask how the affinity of the docking interaction affects enzymatic activity and how to pick the optimal interaction module to complement a given substrate. Here, we develop equations that predict the optimal binding strength of a kinase docking interaction and validate it using numerical simulations and steady-state phosphorylation kinetics for tethered protein kinase A. We show that a kinase–substrate pair has an optimum docking strength that depends on their enzymatic constants, the tether architecture, the substrate concentration, and the kinetics of the docking interactions. We show that a reversible tether enhances phosphorylation rates most when 1) the docking strength is intermediate, 2) the substrate is nonoptimal, 3) the substrate concentration is low, 4) the docking interaction has rapid exchange kinetics, and 5) the tether optimizes the effective concentration of the intramolecular reaction. This work serves as a framework for interpreting mutations in kinase docking interactions and as a design guide for engineering enzyme scaffolds.

docking interaction | phosphorylation | kinase | tethered catalysis | enzyme kinetics

Protein kinases form the backbone of cellular signaling pathways, where they must distinguish their cognate substrates from a wealth of similar protein sequences. The sequence motif surrounding the phosphorylation site only provides part of this specificity as the peptide motifs elucidated in vitro do not predict substrate usage in vivo. Kinase specificity relies heavily on the local abundance of substrates and enzymes, which means that the same kinase can act in several distinct microenvironments and pathways (1, 2). The local abundance of kinases relies on either protein interaction domains (3) or associated anchoring and scaffolding proteins (4). These protein interactions can tether kinases to upstream activators or downstream substrates in what is referred to as signaling complexes. When the kinase is tethered to its substrate, phosphorylation occurs inside a complex where the substrate is present at high effective concentration (C_{eff}). Such tethering can increase the rate of phosphorylation by orders of magnitude (5–8) and thus increase signaling specificity compared to untethered substrates.

A broad picture of how kinase tethering works has emerged from studies of key model kinases. The active site of the kinase recognizes a short linear motif (SLiM) surrounding the phospho-site. A reasonably good motif is required to position the substrate correctly for phosphorylation, but bona fide substrates are often far from the consensus sequence. Additionally, many kinases use structurally independent docking interactions, which are not required to position the substrate in the active site but rather increase the C_{eff} of the substrate (6). Since precise positioning is not required, the docking interaction can take many forms. MAP kinases and cyclin A:cyclin-dependent kinase 2 recognize SLiMs using a binding pocket distant from the catalytic site (6, 9, 10). Other kinases contain dedicated protein interaction domains that typically bind SLiMs such as SH2 or SH3 domains. The kinase and substrate can also be tethered by other proteins, for example, in the case of protein kinase A (PKA), the family of more than 50 different A-kinase anchoring proteins (AKAPs) (2). Many different connections between kinase and substrate can work, as long as the substrate is sterically allowed to bind while the docking interaction is in place (8). Therefore, signaling complexes often involve intrinsically disordered regions (IDRs) (11) that act as flexible chains and provide the required conformational freedom. The linker architecture also defines the C_{eff} of the tethered substrate, which regulates the phosphorylation reaction via a Michaelis–Menten-like dependence on C_{eff} (5). When the linker is longer than needed, the C_{eff} decreases with linker length following a polymer scaling law, which depends both on the length and chemical composition of the linker (12). In total, the specificity enhancement of kinase tethering thus depends on the interplay between what can be considered three interacting modules, as follows: the substrate motif, the docking interaction, and the linker architecture.

Significance

Many enzymes are tethered to their substrates through reversible interactions that are independent of the catalytic site. The strength of these interactions varies greatly, and docking lifetimes span from milliseconds to hours. We investigate how the strength of the docking interaction affects the enhancement of the enzyme reaction. Using a model system consisting of a kinase tethered to its substrate via disordered linkers, we show that tethered enzymes have an optimal docking strength, where stronger and weaker interactions both reduce catalysis. We derive equations that predict how the optimum depends on the linker architecture, substrate concentration, and enzyme parameters. These equations may be used to interpret the effect of mutations in enzyme-targeting domains and design targeting domains for biotechnology.

Author contributions: M.D., N.S.G.F., and M.K. designed research; M.D., N.S.G.F., and D.E.O. performed research; M.D., N.S.G.F., D.E.O., and M.K. analyzed data; M.D., N.S.G.F., D.E.O., and M.K. wrote the paper.

The authors declare no competing interest.

This article is a PNAS Direct Submission.

[1]M.D. and N.S.G.F. contributed equally to this work.

[2]Present address: Novozymes A/S, Krogshøjvej 36, 2880 Bagsvaerd, Denmark.

[3]To whom correspondence may be addressed. Email: magnus@mbg.au.dk.

This article contains supporting information online at http://www.pnas.org/lookup/suppl/doi:10.1073/pnas.2203098119/-/DCSupplemental.

Published June 13, 2022.

Kinase docking interactions are usually nonconvalent and reversible, and their strength can be characterized by rate and equilibrium constants for binding and dissociation (K_D, k_{on}, and k_{off}). High-affinity AKAPs bind with a subnanomolar K_D (13), whereas SLiMs typically have K_D values in the micro- to millimolar range (14). This translates into complex lifetimes from many minutes to milliseconds. Catalytic efficiency has a nontrivial dependence on docking strength, as stronger docking interactions have either been found to decrease (7) or increase (8) steady-state phosphorylation by cyclin-dependent kinase and the same docking interaction affects substrates differently (15). This has led to the general conclusion that docking interactions should have a moderate affinity (16) in analogy with the Sabatier principle in heterogeneous catalysis (17, 18). The kinetic origins of this principle are illustrated by considering the extremes of strong and weak docking. Weak docking leads to little complex formation and thus does not enhance phosphorylation rates above the untethered reaction. Strong binding saturates the enzyme with substrate and allows an efficient first cycle of phosphorylation. However, subsequent catalytic cycles are limited by slow product dissociation and thus reduced k_{cat}. Enzyme docking interactions are prone to this type of product inhibition, as the binding site is structurally independent from the substrate and does not change in the reaction. Efficient docking interactions must be of intermediate strength to be sufficiently strong to ensure a reasonable bound population and sufficiently weak to allow rapid product dissociation.

What does an optimum at an intermediate binding strength mean in practice? Also, how does it depend on the properties of the substrate and linker architecture? These are not just questions of fundamental interest but have practical implications in the design of synthetic signaling scaffolds (19) or the interpretation of disease-associate mutations in kinase anchoring proteins. Increased docking strength can either increase or decrease the activity of a pathway, although this cannot be predicted currently even when the molecular details are known. Here, we aim to develop a kinetic framework for predicting how kinase tethering affects steady-state phosphorylation rates depending on the properties of the substrate motif, the docking interaction, and the linker architecture. A key goal is to define the optimal docking strength for a system as it allows us to predict whether catalytic efficiency increases or decreases with increased affinity.

Many kinase tethering systems have a modular design with flexibly linked docking interactions. Therefore, it is likely possible to develop a kinetic framework that describes many different kinases or even other classes of similarly tethered enzymes such as phosphatases (20). The generality of the approach taken here rests on the assumption that the transient connection between enzyme and substrate only acts as a passive linker that defines C_{eff}. Some docking motifs also affect catalytic efficiency through allostery (21–23), whereas others can be accounted for through steric effects (24). In general, allosteric effects are most likely for direct docking to the catalytic domain and unlikely for docking via protein interaction domains and linkers as used here. Sequence–function relationships among IDRs are complex, but the assumption of a passive linker is a good baseline hypothesis for many systems, as demonstrated by the successes in describing IDRs using polymer models (25).

A general kinetic scheme can be studied in a convenient model system such as PKA, which is well-described in terms of structure, mechanism, and kinetics. The catalytic mechanism is similar in other kinases and is well captured by standard kinetic descriptions. The key challenge is thus how to represent the structurally diverse connection between kinase and substrates in a way where the properties of the connection can be continuously varied and quantified. We recently developed a model system to study single-turnover reactions of tethered PKA, where the kinase is connected to the substrate via two disordered linkers connected by a heterodimeric coiled-coil (Fig. 1*A*). The connection can be continuously tuned by changing the lengths of the linkers, which were kept strictly as glycine-serine repeats to avoid sequence-specific effects (5). Here, we expand this model system by varying the strength of the coiled-coil interaction more than 1,000-fold and investigate how steady-state phosphorylation by reversibly tethered PKA depends on the properties of the substrate, the docking interaction, and the linker architecture. Numerical simulations and experiments are used to validate analytically derived rate equations that provide a general framework to predict the effects of enzyme tethering.

Materials and Methods

Preparation of DNA Constructs. Plasmids were prepared by de novo synthesis by Genscript and codon optimized for expression in *Escherichia coli*. The coding regions were cloned into pET15b vectors using the NdeI/XhoI sites. The protein sequences and the list of all constructs used are given in *SI Appendix*.

Protein Expression and Purification. The MBD2 peptide containing an N-terminal His-tag and a single C-terminal cysteine (MBD2-Cys) was expressed in BL21(DE3) cells in ZYM-5052 autoinduction medium containing 100 μg/mL ampicillin at 37 °C and shaking at 120 rpm for 22 h. The cells were harvested by centrifugation (15 min, 6,000 × g), and bacterial pellets were resuspended in a binding buffer (20 mM NaH_2PO_4, 0.5 M NaCl, 20 mM imidazole, 0.1 mM TCEP [pH 7.4]). To lyse the cells and precipitate folded proteins, the cell suspension was incubated for 25 min at 80 °C, while shaking at 400 rpm, before the cell suspension was rapidly cooled on ice (26). The lysate was centrifuged (15 min, 27,000 × g), and the supernatant was applied to gravity flow columns packed with Ni-NTA Superflow (QIAGEN). The columns were washed with buffers (20 mM NaH_2PO_4, 0.5 M NaCl, 0.1 mM TCEP) containing increasing concentrations of imidazole (40, 60, 80, 100, 200, and 500 mM). A sodium dodecyl sulfate–polyacrylamide gel electrophoresis (SDS-PAGE) gel revealed purified MBD2 peptide in fractions containing 200 and 500 mM imidazole. These fractions were dialyzed against TBS buffer (20 mM Tris-base, 150 mM NaCl, 0.1 mM TCEP [pH 7.6]) and subsequently supplemented with trifluoroacetic acid (TFA) to bring the pH to 2, before an additional purification step by reverse-phase chromatography in 0.065% TFA buffer, with elution buffer also containing 70% acetonitrile, and using SOURCE 15RPC ST 4.6/100 column (Cytiva). Eluted fractions were lyophilized to dryness.

Protein constructs containing the catalytic domain of PKA linked by a $(GS)_n$-linker to the MBD2 coiled-coil domain (MBD2-$(GS)_n$-PKAc, with n = 10, 30, or 60) and an N-terminal His-tag were expressed in C41(DE3) cells in LB medium with 100 μg/mL ampicillin at 37 °C and shaking at 120 rpm. The cultures were induced with 1 mM IPTG at an optical density at 600 nm (OD_{600}) of ∼1, and the temperature was decreased to 20 °C for an overnight expression. The cells were harvested by centrifugation (15 min, 6,000 × g), and bacterial pellets were resuspended in binding buffer (20 mM NaH_2PO_4, 0.5 M NaCl, 5 mM imidazole, 0.1 mM TCEP, 0.2 mM PMSF, 50 mg/L of leupeptin, 50 mg/L pepstatin, 50 mg/L chymostatin [pH 7.4]) and lysed by sonication (50% duty cycle, maximum power of 70%, sonication time of 5 min). The lysates were centrifuged (20 min, 27,000 × g), and the supernatants were applied to gravity flow columns packed with Ni-NTA Superflow (QIAGEN). The columns were washed with buffers (20 mM NaH_2PO_4, 0.5 M NaCl, 0.1 mM TCEP) containing increasing concentrations of imidazole (20, 30 and 40, 150, and 500 mM). SDS-PAGE gels revealed purified PKA samples in fractions containing 40 and 150 mM imidazole. These fractions were upconcentrated (Vivaspin 20 concentrators, 10,000 molecular weight cut-off (MWCO)) and additionally purified by size-exclusion chromatography (SEC) in TBS buffer using the Superdex 75 Increase column (Cytiva).

Protein constructs containing PKA substrates (wild type [WT], R-2K, or R-3K) linked to the p66α coiled-coil domain (p66α-QS-substrate, with 6 variants of p66α) and an N-terminal His-tag were expressed in BL21(DE3) cells in Terrific broth (TB) medium containing 100 μg/mL ampicillin at 37 °C and shaking at

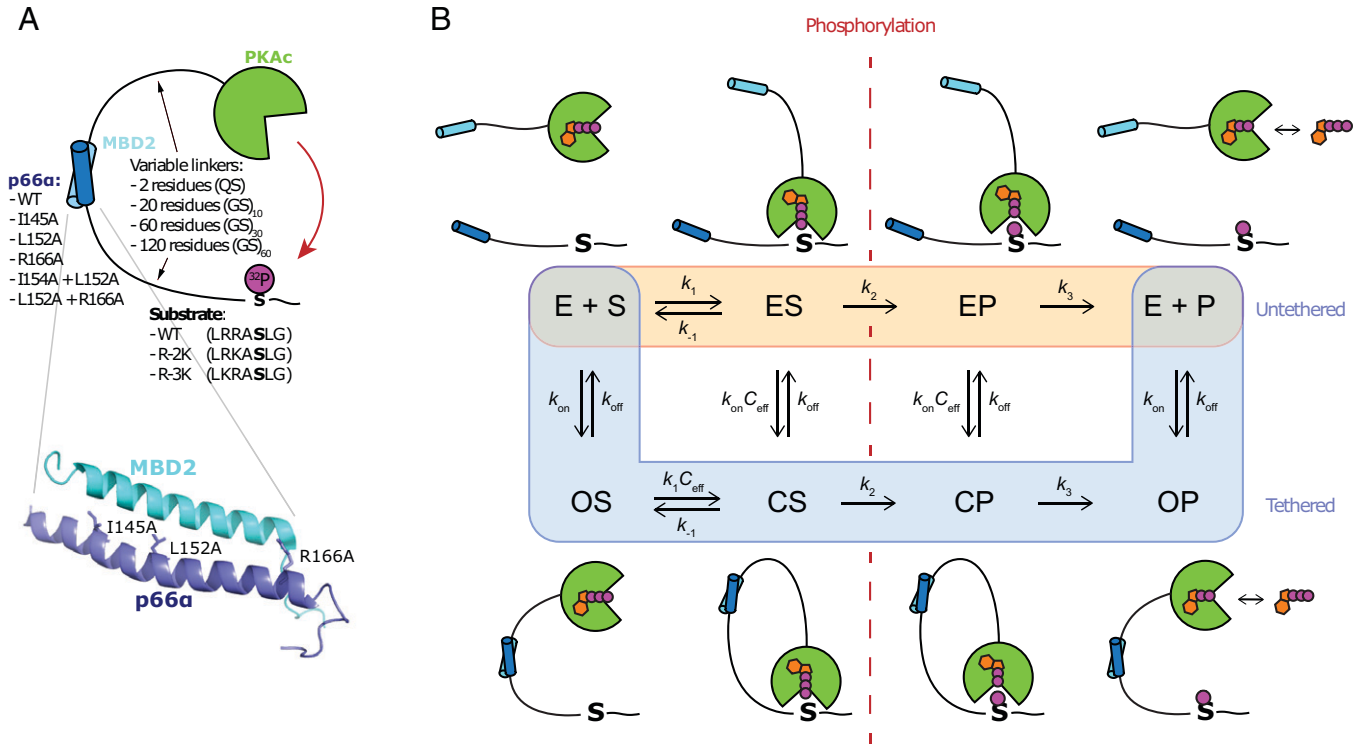

Fig. 1. A model system for reversible tethered kinases. (*A*) The model system (5) consists of the catalytic domain from PKA (PKAc) tethered to different substrate motifs via the coiled-coil interaction between p66α and MBD2 (PDB: 2L2L) (31) and disordered GS linkers. The model system is extended by varying the strength of the docking interaction by mutagenesis of p66α. (*B*) Kinetic scheme of the main reaction pathways, where the substrate is either phosphorylated by a tethered or untethered kinase. This scheme omits the ternary complex pathway (*SI Appendix*, Fig. S1) that is kinetically less important. ADP and ATP are represented as orange symbols with phosphates in purple but are not explicitly included in the model. E, S, and P denote the free enzyme, substrate, and product. ES and EP denote states where the active site is bound to a substrate or product without binding to the docking interaction. OS and OP represent states where the enzyme is docked to substrate and product in open conformations, and CS and CP are the corresponding closed conformations.

120 rpm. After induction with 1 mM IPTG at an OD_{600} of ∼0.9, the cultures were allowed to grow for 4 h at 37 °C. The cells were harvested by centrifugation (15 min, 6,000 ×g), and bacterial pellets were resuspended in binding buffer (20 mM NaH_2PO_4, 0.5 M NaCl, 5 mM imidazole [pH 7.4]). To lyse the cells and precipitate folded proteins, the cell suspensions were incubated for 25 min at 80 °C, while shaking at 400 rpm, before the cell suspension was rapidly cooled on ice. The lysates were centrifuged (15 min, 27,000 ×g), and the supernatants were applied to gravity flow columns packed with Ni-NTA Superflow (QIAGEN). The columns were washed with buffers (20 mM NaH_2PO_4, 0.5 M NaCl, 0.1 mM TCEP) containing 20 mM of imidazole and eluted with 500 mM imidazole. Elution fractions were upconcentrated (Vivaspin 20 concentrators, 5,000 MWCO) and dialyzed against TBS buffer.

Labeling of MBD2 Peptide. For stopped-flow experiments, 100 μM of the MBD2-Cys peptide in TBS buffer was reduced in 1 mM TCEP and subsequently labeled with 2 mM maleimide-activated dansyl dye (Sigma-Aldrich) at 4 °C overnight, protected from light, and with 15 rpm rolling. The reaction was stopped with 52.7 mM β-mercaptoethanol, and excess dye was removed by SEC in TBS buffer using Superdex 75 Increase column (Cytiva).

Stopped-Flow Measurements. Binding kinetics of the docking interaction MBD2/p66α were measured using a Chirascan spectrometer equipped with a Hg-Xe lamp with a stopped-flow mixing accessory (Applied Photophysics) and monitoring dansyl fluorescence. Excitation was at 334 nm with a 10-nm bandwidth, and a 495-nm long pass filter was used to monitor the emission. Measurements were done at 30 °C in TBS buffer. In order to obtain observed association rate constants (k_{obs}), MBD2-Cys-dansyl at a constant concentration of 100 nM was mixed with an equal volume of 2.5 to 20 μM of p66α-QS-substrate^{WT}. For the lowest affinity p66α$^{I145A+L152A}$-QS-substrate^{WT} mutant, higher concentrations of 12.5 to 100 μM were used to improve the amplitude of the kinetic trace. The traces were fitted with a single exponential association model to obtain k_{obs}, observed rate constants were plotted versus p66α concentrations, and the data were fitted by linear regression to determine the second-order association rate constant (k_{on}) from the slope of the fitting line. Dissociation rate constants were determined through displacement experiments by first mixing 100 nM of MBD2-Cys-dansyl with 1 μM of p66α-QS-substrate^{WT}, followed by mixing the preformed complex with an excess (5 μM) of unlabeled MBD2-Cys that competes for binding to p66α such that MBD2-Cys-dansyl is mostly unbound at equilibrium. For p66α mutants with low affinity (p66α$^{I145A+L152A}$-QS-substrate^{WT} and p66α$^{L152A+R166A}$-QS-substrate^{WT}), higher concentrations were used to improve the amplitude of the kinetic trace (10 μM of p66α-QS-substrate^{WT} and 50 μM of unlabeled MBD2-Cys). The traces were fitted with a single exponential dissociation model, and the observed rate constants are equal to k_{off}.

Numerical Simulations. Numerical simulations were performed using KinTek Global Kinetic Explorer software (27) based on a full kinetic model including four reaction pathways, as follows: untethered, tethered (Fig. 1*B*), and two ternary pathways (*SI Appendix*, Fig. S1). An editable mechanism file can be found online at doi:10.6084/m9.figshare.19620720. The association rate of the docking interaction was chosen to match WT MBD2:p66α ($k_{on} = 1.8 \times 10^7\ s^{-1}\ M^{-1}$), and k_{off} was varied from 0.001 to 1,000 s^{-1}. The rate of phospho-transfer (k_2) was set at saturation rate measured by single-turnover kinetics of the tethered reaction (WT: 307 s^{-1}, R-2K: 40 s^{-1}, R-3K: 14.1 s^{-1}) (5). The association rate constant of all substrates was set at a value typical of SLiMs ($k_1 = 10^7\ s^{-1}\ M^{-1}$). The substrate dissociation rate constant (k_{-1}) was varied such that the resulting $K_D = k_{-1}/k_1$ matches the observed half-saturation point of the tethered phosphorylation reaction (WT: 1420 s^{-1}, R-2K: 8370 s^{-1}, R-3K: 84,000 s^{-1}). ADP release is the rate limiting product dissociation step for PKA (28) and was estimated to ($k_3 = 42\ s^{-1}$) based on the steady-state kinetics of WT substrate and applied to all substrates. To test the effect of substrate concentration, all three substrates were simulated at concentrations ranging from 0.1 to 100 μM at a fixed C_{eff} of 388 μM corresponding to the longest linker used in this study (see below). To test the effect of linker length, C_{eff} was varied between 30 and 3000 μM for a fixed concentration of 3 μM of all substrates. To ensure that no more than 10% of the initial substrate was converted to product, the reactions were simulated for reaction time of 300 s with enzyme concentrations at 10 pM. The formation of all

phosphorylated reaction species (EP+P+CP+OP+OSP+OPP) in time was subjected to linear regression, and the reaction rate was measured from the slope and converted to specific activity by division with the enzyme concentration.

C_{eff} Calculations. Our tethered kinase systems provide complex linker architectures between the kinase and substrate that consist of flexible segments of 20, 60, or 120 GS residues from the enzyme construct, glutamine-serine plus extra residues from the substrate construct, and a folded coiled-coil p66α-MBD2 heterodimer. To calculate C_{eff} covering this complexity, a newly developed approach based on conformational ensembles was used (29). Briefly, a physically realistic ensemble of the linker was modeled using the Ensemble Optimization Method (EOM). As EOM cannot handle heterodimers, the p66α-MBD2 coiled-coil was replaced with a α-helical poly-alanine rod, which has a similar length and produces the same end-to-end distribution as the folded domain (29). Flexible segments were simulated as beads using the Native chain for an ensemble of 10,000 conformations. The flexible segments were defined from the first residue not defined in the Protein Data Bank (PDB) structures of the PKAc (PDB: 2CPK) or the p66α:MBD2 coiled-coil (PDB: 2L2L) and the first residue in the consensus substrate motif. As the flexible linkers are attached to the C terminus of both coiled-coil segments, the sequence of the linker between the kinase domain and the substrate domain were set in backward in the EOM simulation. End-to-end distribution and C_{eff} were then calculated for a spacing of 34 Å, which is the distance the linker architecture must span between the active site and the N-terminal attachment site of the PKA catalytic domain (*SI Appendix*, Fig. S3).

Steady-State Kinetics. A given PKAc construct linked to the MBD2 coiled-coil domain (MBD2-$(GS)_n$-PKAc) was diluted to 10× final concentration in enzyme dilution buffer (50 mM Tris-base, 0.1 mM EGTA, 1 mg/mL bovine serum albumin, 1 mM TCEP [pH 7.6]), and a p66α-QS-substrate was diluted to 10× final concentration in TBS buffer. Steady-state experiments were executed by manual addition of [γ-^{32}P]ATP (final concentration of 0.1 mM of 100 to 200 c.p.m. $pmol^{-1}$) into a reaction mix containing 0.2 or 1 nM MBD2-$(GS)_n$-PKAc and p66α-QS-substrate (final concentration of 1, 3, and 10 μM) in a reaction buffer (50 mM Tris-base, 0.1 mM EGTA, 10 mM magnesium acetate, 150 mM NaCl [pH 7.6]) at 30 °C. In evenly distributed time-steps (20, 30, or 60 s) 30 μL of the reaction mix was spotted onto a 4-cm^2 P81 filter disk (Jon Oakhill, St. Vincents Institute of Medical Research) and placed into 75 mM phosphoric acid to quench the reaction. The filters were washed three times with 75 mM phosphoric acid, rinsed with acetone, dried, and counted on the ^{32}P channel in scintillation counter as c.p.m. Control experiments were performed in similar manner, using TBS buffer instead of substrate in the reaction mix. These procedures were performed in triplicate. Initial velocities were derived from a slope of a linear regression as micromolar of ^{32}P-incorporated to substrate per minute. Phosphorylation rates (V_0/E_0) were then calculated by dividing the slope by the final concentration of PKAc for each experiment (*SI Appendix*, Figs. S4–S9).

Results

We recently developed a model system to study tethered phosphorylation reactions by single-turnover kinetics (5). The system (Fig. 1*A*) is composed of two parts, as follows: the catalytic domain of PKA linked to the MBD2 coiled-coil domain via a flexible Gly-Ser linker of variable length and a substrate derived from Kemptide (30) linked to the coiled-coil domain from p66α. The MBD2 and p66α domains associate to form a heterodimeric coiled-coil with nanomolar affinity (31). The strong docking interactions between the WT domains lead to a lifetime of the complex that is much longer than the rate of intramolecular phosphorylation and the reaction is effectively single turnover at short timescales. Therefore, this system mimics both high-affinity docking interactions and permanent covalent tethering to intramolecular substrates. Weaker docking interactions lead to multiple association–dissociation events within the experimental time frame. Consequently, phosphorylation can occur through several parallel pathways. The most important pathways are the untethered and bimolecularly tethered pathways shown in Fig. 1*B*, which differ in whether the docking interaction is formed. Additionally, the reaction can occur through a ternary complex, where a tethered kinase phosphorylates a different substrate from the one it is tethered to (*SI Appendix*, Fig. S1).

To adapt this model system to study reversibly tethered kinases, we wanted to vary the strength of the docking interaction, while keeping other parameters constant. We mutated three residues in the coiled-coil interface (Fig. 1*A*) to alanine to destabilize the complex. We characterized the association and dissociation kinetics of these variants to a fluorescently labeled MBD2 peptide (Fig. 2 and *SI Appendix*, Fig. S2) using stopped-flow fluorimetry. The WT interaction has a K_D of 4.2 nM that is in agreement with previous studies (31) and a fast association ($k_{on} = 1.8 \times 10^7\ M^{-1}s^{-1}$) typical of IDP interactions (*SI Appendix*, Table S1). Single point mutations increased the K_D by up to 61-fold, and their combination into two double mutants further increased K_D up to ∼2,400-fold. This reduction of the docking interaction strength occurred mostly through increased k_{off} values, which rose by ∼500-fold compared to less than 5-fold reduction of the k_{on} values (*SI Appendix*, Table S1). This was expected as association rates often fall in a relatively narrow range in the absence of electrostatic steering or rate-limiting structural changes (32).

We performed numerical simulations to generate theoretical predictions for reversibly tethered kinases and considered the following four reaction pathways: untethered, tethered (both shown in Fig. 1*B*), and two kinds of ternary complexes where the kinase is attached to a phosphorylated or unphosphorylated substrate (*SI Appendix*, Fig. S1). We simulated phosphorylation of three different variants of the Kemptide substrate, as follows: the original Kemptide (WT), which is the optimal substrate for PKA, and two point mutations that reduced k_{cat}/K_M by ∼10 (R-2K) and ∼100-fold (R-3K) (5), thus comprising a good, an intermediate and a poor substrate. We fixed the k_{on} of the docking interaction at the value for WT MBD-p66α ($k_{on} = 1.8 \times 10^7\ M^{-1}s^{-1}$), which will be similar for many small linear motifs, and varied k_{off} to represent docking interactions of various strengths. Recently, we developed a method for estimating the C_{eff}s of linkers containing rigid elements such as coiled-coil used here (29). The C_{eff} was determined from an ensemble of 10,000 conforms where MBD2:p66α is simulated as a rigid rod, and disordered segments are treated as a random chain (*SI Appendix*, Fig. S3). This method resulted in a lower dependence of C_{eff}s on linker length than previous estimates. Furthermore, the shortest linker length used previously did not increase C_{eff}s and was thus not included in this study (5). For the 120-residue GS-linker, this resulted in a calculated C_{eff} of 388 μM, which was used as a baseline in numerical simulations. The numerical simulations predict that steady-state phosphorylation rates have a bell-shaped dependence on the docking strength (k_{off}) for substrate concentrations from 0.1 to 100 μM (Fig. 3 *A*–*C*). At high or low docking strengths, the total rate approaches the untethered rate but reaches an apex at intermediate k_{off} values. At higher substrate concentrations, the apex shifts toward weaker docking interactions and the peak broadens. The baseline increases for high substrate concentrations and for better substrates. This is expected as the K_M of Kemptide is in the low micromolar range (5, 28) and is thus similar or above the substrate concentration. Accordingly, the flux through the pathways that are independent of the tethering strength, i.e., the untethered and ternary routes, increases.

We then sought to develop an analytical solution that could allow us to identify the factors governing the shape and the position of the apex of the bell curves in Fig. 3 *A*–*C*. It is impractical to consider all four reaction paths in the rate equations, so we inspected the numerical simulations to find

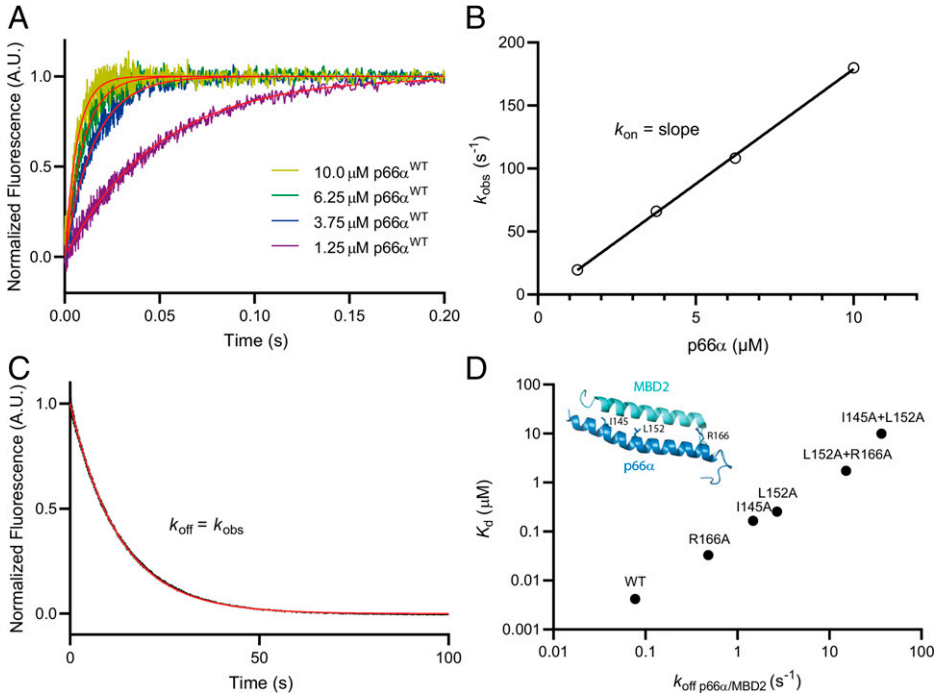

Fig. 2. Binding kinetics of variants of the p66α-MBD2 docking interaction by stopped-flow. (*A*) Binding of p66α to 50 nM dansyl-labeled MBD2 under pseudo-first order conditions. (*B*) The observed rate constant of the fluorescence signal depended linearly on the concentration of p66α with a slope of k_{on}. (*C*) Displacement of 50 nM of dansyl-labeled MBD2 by 2.5 mM of unlabeled MBD2 from a limiting concentration (0.5 mM) of p66α. The observed rate constant is independent of the competitor concentration, which indicates that the observed rate corresponds to a k_{off}. (*D*) The excellent correlation (R = 0.97) between dissociation constants and k_{off} in the p66α variants shows that the complex is mainly stabilized through a slower dissociation. Error bars representing the SE from the fit are smaller than the symbols.

reaction paths that could be omitted. The simulations indicated that at low substrate concentrations, the ternary and untethered reaction paths could be ignored. This can be rationalized based on the diffusion-limited access to substrate under these conditions. Therefore, we based our derivation exclusively on the tethered reaction path (Fig. 1*B*). We derived a kinetic rate equation for product formation under steady-state conditions as a function of the dissociation rate k_{off} (*SI Appendix*):

$$\frac{dP}{dt} = \frac{a}{bk_{off} + \frac{c}{k_{off}} + d} \quad [1]$$

Where a, b, c, and d are constants that depend on S_0, E_0, C_{eff}, k_{on}, k_1, k_{-1}, k_2, and k_{-3} as defined in *SI Appendix*. Comparison of predicted kinetics from Eq. **1** to the numerical simulations (Fig. 3 *A*–*C*) reveals that Eq. **1** describes the reaction kinetics well at low concentrations but underestimates the phosphorylation rate due to increased flux through the untethered and ternary paths at higher substrate concentrations. However, Eq. **1** still correctly describes the position of the apex seen in the numerical simulations despite significant flux through the untethered path as well as the general behavior of the curve as concentration varies. This observation led us to further calculate the derivative of Eq. **1** relative to k_{off}, to obtain an expression for docking strength that results in the fastest phosphorylation rate, k_{off_apex} (*SI Appendix*):

$$k_{off_{apex}} = \sqrt{\frac{k_{on}\, k_1\, k_2\, C_{eff}\, S_0}{k_{-1} + k_2}} \quad [2]$$

Which for enzymes that follow the Michaelis–Menten reaction scheme (where $k_2 = k_{cat}$ and $K_M = (k_{-1} + k_2)/k_1$) can be simplified to:

$$k_{off_{apex}} = \sqrt{\frac{k_{cat}}{K_M}\, k_{on}\, C_{eff}\, S_0} \quad [3]$$

The apex separates two regimes where the strength of the docking interaction affects the catalytic efficiency in opposite directions; at low k_{off} values (high docking strength), the docking lifetime is longer than the time required for catalysis. Most docking events lead to phosphorylation, and the reaction is limited by how fast the product can be released. Therefore, this region is insensitive to the substrate concentration as kinase is saturated with substrate and flux through untethered and ternary paths are negligible. At higher k_{off} values (low docking strength), docking events are shorter than the time required for full phosphorylation, which means that product dissociation is no longer limiting. Instead, the reaction is limited by the fraction of enzymes bound to substrates via the weak docking interaction. Eqs. **2** and **3** describe the cross-over between these regimes, and they can be calculated from parameters that can either be measured using standard assays or predicted from physical models.

To test the numerical simulations, we performed a series of steady-state phosphorylation experiments using MBD2-$(GS)_{120}$-PKAc as the enzyme and p66α-QS-substrates. For each substrate, we tested our six docking variants at substrate concentrations where the tethered route was predicted to be important corresponding to the middle concentrations used in numerical simulations (1 and 10 μM) and an intermediate concentration of 3 μM (Fig. 3 *D*–*F* and *SI Appendix*, Figs. S4–S6). Steady-state phosphorylation rates have a bell-shaped dependence on the docking strength for the poor and intermediate (R-3K and R-2K) substrates, whereas no clear apex is seen for the optimal (WT) substrate. Eq. **2** shows that the apex for the optimal substrate is expected at higher k_{off} values than those covered by the range of docking strengths tested. The WT substrate is efficiently phosphorylated regardless of the docking strength with values similar to an untethered reaction (Fig. 3*F*). A similar situation is seen in the numerical simulations (Fig. 3*C*), where a small increase is observed on top of a high base line due to a high flux through the nontethered reaction paths. For the suboptimal substrates, the rates are greatly enhanced and only approach the baseline at high

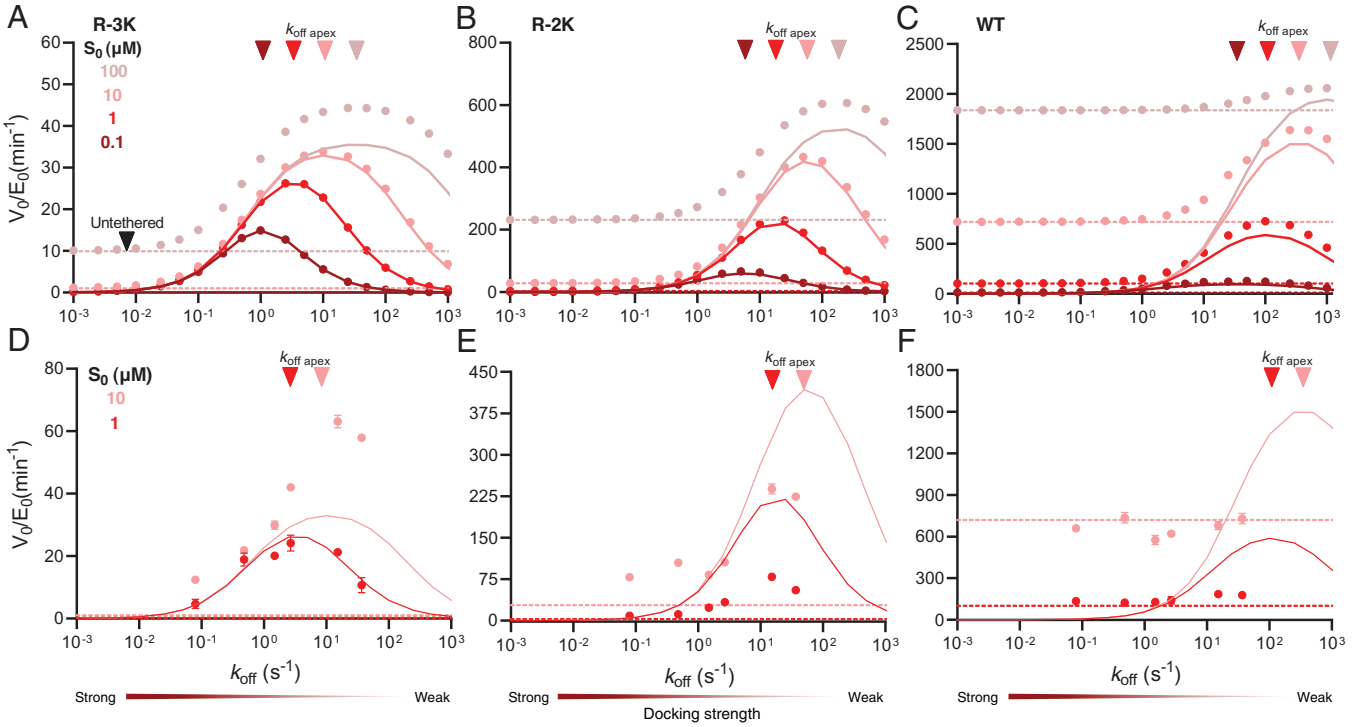

Fig. 3. Steady-state phosphorylation rate dependency on substrate concentration from numerical simulations and experiments. (*A–C*) Numerical simulation (solid circles) of the steady-state phosphorylation rates for three different PKA substrates, namely, R-3K (*A*), R-2K (*B*), and WT (*C*), at different concentrations. The k_{cat}/K_M of the substrates increase 10-fold from R-3K to R-2K and from R-2K to WT. The simulations include the tethered, untethered (Fig. 1*B*), and ternary reaction paths (*SI Appendix*, Fig. S1). The k_{on} was fixed to 1.8 × 10^7 M^{-1} s^{-1} corresponding to MBD2/p66α and the C_{eff} at 388 μM corresponding to a 120-residue GS linker. Rate constants for the substrates are based on previous studies (5). The dashed lines depict the simulated rates from the untethered reactions with identical parameters (i.e., a parameter that only varies with substrate concentration, not k_{off}), and the solid lines represent predicted rates from a reaction that only proceeds through the tethered route based on Eq. **1**. Solid triangles indicate the value of k_{off_apex} calculated by Eq. **2** (which is based on Eq. **1**) at the simulated conditions. (*D–F*) Experimental steady-state phosphorylation rate values for R-3K (*D*), R-2K (*E*), and WT (*F*) substrates at three different substrate concentrations. Error bars represent the SEM, with $n = 3$. Solid triangles indicate the value of $k_{off,apex}$ calculated using Eq. **2** for experimental conditions. Unless indicated otherwise, parameters in *D–F* are identical to *A–C*.

or low k_{off}. The baseline is defined by the untethered reactions and increase for better substrates and at higher substrate concentrations.

The predicted position of the apex from Eq. **2** varies ∼30-fold from the poor to the best substrate (R-3K: k_{off_apex} ∼3 to 10 s^{-1} and WT: $k_{off,apex}$ ∼100 to 300 s^{-1}) and a factor of 3.2 between the highest and lowest measured concentrations (Fig. 3 *D–F*). For both R-3K and R-2K, the predicted apex falls between the two highest observed rates for all concentrations. The change in apex following a 10-fold increase in concentration is less than the spacing between data points and is thus seen as a shift in the relative intensity of the fastest rates. Across this variation of substrate quality and concentration, Eqs. **2** and **3** predict the position of the apex within a factor of ∼2 to 3 despite of the approximations made, thus revealing the predicting capabilities of the analytical solutions.

Eq. **1** also predicts the magnitude of the rate enhancement due to tethering. We found a general agreement between experimental and predicted rate, although minor disparities are observed in the amplitudes, for example, for R-3K at high concentrations. These differences could be explained by slightly different values of the rate constants that govern substrate binding to the active site (k_1, k_{-1}) while keeping a constant k_{cat}/K_M ratio (*SI Appendix*, Fig. S10). Further assessments of the accuracy and predicting potential of our general equations led us to calculate Eq. **1** using parameters C_{eff} = 388 μM and [S_0] = 1, 3, and 10 μM as in our experimental setup (*SI Appendix*, Fig. S11). Eq. **1** appropriately describes the experimental steady-state rate behavior for R-3K and less effectively for the WT substrate due to the dominance of the untethered route not considered in the model.

The connection between kinases and their substrates controls the C_{eff} of the intracomplex substrate binding interaction and thus impacts the kinetics of the single turnover reaction. However, good substrates are subject to saturation of their single turnover rates in a Michaelis–Menten-like dependence on the C_{eff}. This implies that there is a regime where a change in the linker architecture will not affect the rate of phosphorylation. We wanted to test whether transiently tethered kinases are subject to a similar form of C_{eff} saturation. In PKA-AKAP signaling complexes, the C_{eff} is estimated to vary from the low millimolar to hundreds of micromolar (33). We thus performed numerical simulations and compared the three different substrates at a range of C_{eff}s that varied from 30 μM to 3,000 μM. We simulated the phosphorylation reaction at a 3 μM substrate concentration and fixed association and dissociation rate constants as previously described (Fig. 4 *A–C*). Unlike changes in substrate concentration, changes in C_{eff} will usually not influence the flux of the phosphorylation reaction through nontethered pathways. The relative impact of C_{eff} changes is more significant for the poor substrate R-3K; an increase from 300 μM to 3 mM increases phosphorylation rates 5.1-fold at the apex value for R-3K but only ∼1.2-fold for the WT substrate. This is reminiscent of the Michaelis–Menten-like dependence observed for tethered single-turnover phosphorylation rates and occurs for the same reason. For the good WT substrates, the tethered substrate binds fully to the kinase, and increases in C_{eff} do not increase the fraction of catalytically competent closed complex in contrast to weaker substrates. In addition, as predicted by Eq. **2**, lower C_{eff} (longer linkers) pushes the apex toward stronger binding interactions (lower k_{off_apex}) for all substrates.

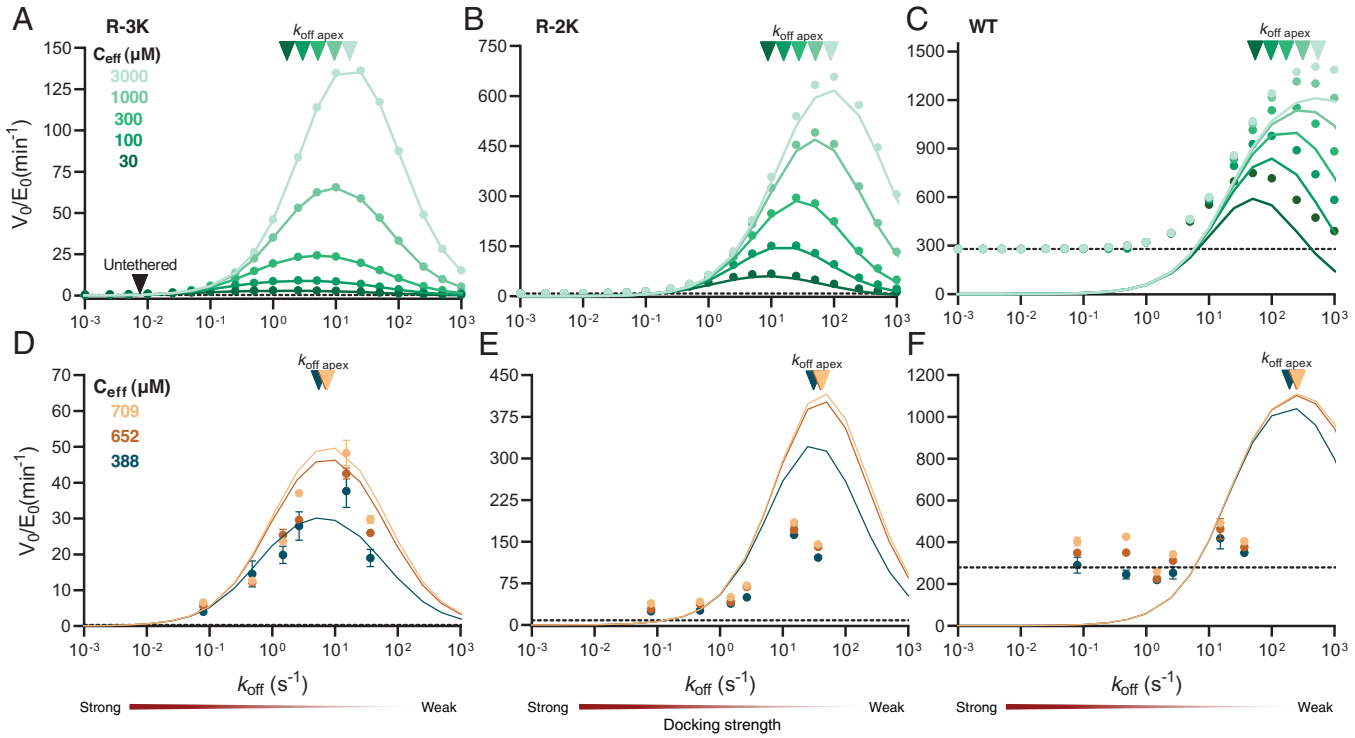

Fig. 4. Steady-state phosphorylation rate dependency on C_{eff} from numerical simulations and experiments. (*A–C*) Numerical simulation (solid circles) of the steady-state phosphorylation rate at different C_{eff}s for R-3K (*A*), R-2K (*B*), and WT (*C*) PKA substrates. The simulations include the tethered, untethered, and ternary reaction paths. The substrate concentration was set to 3 μM, and k_{on} and rate constants values for the substrates were fixed as explained in Fig 3. The dashed lines depict the simulated rates from the untethered reactions with identical parameters, and the solid lines represent predicted rates from a reaction that only proceeds through the tethered route based on Eq. **1**. Solid triangles indicate the value of $k_{off,apex}$ calculated by Eq. **2** with all parameters used in the simulations. (*D–F*) Experimental steady-state phosphorylation rate values at three different C_{eff} = 709, 564, and 388 μM, which correspond to a 20-, 60-, and 120-residue GS linker, respectively, for R-3K (*D*), R-2K (*E*), and WT (*F*) substrates. Error bars represent the SEM, with n= 3. Solid triangles indicate the value of $k_{off,apex}$ calculated using Eq. **2** for experimental conditions. Unless indicated otherwise, parameters in *D–F* are identical to *A–C*.

To assess these predictions, we also performed steady-state phosphorylation experiments varying the C_{eff}. Changes in C_{eff} correspond to variations in the connections between enzyme and substrate, which translates into changes in the linker length in our experimental setup. We chose p66α-QS-substrates and three different enzyme constructs, as follows: MBD2-$(GS)_n$-PKAc with $n = 10$, 30, or 60 and estimated C_{eff} values of 709, 652 ,and 388 μM, respectively (*SI Appendix*, Fig. S3). As in the concentration series, we tested docking interaction variants for each substrate quality at a substrate concentration of 3 μM (Fig. 4 *D–F* and *SI Appendix*, Figs. S7–S9). Experiments show that phosphorylation rates vary accompanying changes in C_{eff} with a relative effect that depends on substrate quality and that is more pronounced for k_{off} values near the apex. However, the observed changes are rather small since the range of C_{eff} experimentally tested was limited to only a ∼2-fold change in C_{eff} from the shortest to the longest linker. This range is smaller than in a previous study (5) due to the combined effects of a method of estimation of C_{eff} (29) and exclusion of the shortest and longest linker combination due to steric clashes and protein quality issues, respectively. For the poor substrate, this change in C_{eff} is expected to represent an ∼1.7-fold change in the steady-state rates, whereas for the best substrate has only an ∼1.07-fold change (*SI Appendix*, Fig. S11). The position of the apex (k_{off_apex}) has a square-root dependence on C_{eff} (Eq. **2**), explaining why for our experimental ∼2-fold C_{eff} change we observed a small difference in the position in a factor of 1.4. Regardless of these small changes, the observed general behavior follows predictions by simulations. For the WT substrate, the observed differences in phosphorylation rates are not due to changes in C_{eff} but to experimental error, as they assume values near the predicted untethered rate (Fig. 4*B*).

A given interaction docking strength (K_D) can be achieved by different k_{on}/k_{off} combinations. Using Eq. **1**, we calculated the phosphorylation kinetics at association rates ranging from 10^5 to 10^9 M^{-1} s^{-1}. At comparable K_D values, fast association-dissociation reactions are more efficient at enhancing the kinase because the higher dissociation rate allows it to evade the product inhibition that otherwise limits high-affinity docking interactions (*SI Appendix*, Fig. S12). This effect is less pronounced for poor substrates as phospho-transfer becomes rate limiting instead of substrate dissociation. This prediction is difficult to test experimentally as mutations predominantly change the k_{off} rate, but it explains why enzyme targeting often occurs via SLiMs, which often have higher basal association rates than interactions between two folded domains (34, 35).

Discussion

We have developed a quantitative model of docking interactions for kinases, which captures the kinase targeting through reversible protein interactions. We compared the model to steady-state phosphorylation in a minimalistic model system, which allowed us to vary docking affinity 2,400-fold, the catalytic efficiency of the substrate up to 100-fold, and C_{eff} ∼2-fold. Steady-state kinetics suggest that these parameters affect the phosphorylation reaction by shifting the optimal docking strength and the magnitude of rate enhancement in tethered kinases. The main features of the steady-state kinetics are reproduced by numerical simulations and an equation derived for the tethered reaction path. We suggest that

these equations may serve as a first approximation of the effect of mutations and for designing scaffolding interactions.

The equations derived for the tethered reaction path predict how the optimal docking strength depends on the properties of the kinase:substrate complex. Comparisons to steady-state phosphorylation rates show that the equation predicts apex well for the two weaker substrates, whereas the optimal substrate is predicted to have an apex outside the range of docking strengths tested and is accordingly not observed. When compared to numerical simulations, the analytical equations predict the apex precisely, whereas there are up to t3-fold deviations when compared to experiments. This shows that given precisely defined parameters, the equation predicts the apex exactly. Therefore, the deviations are mainly due to the uncertainty in the parameters. However, an error of a factor of 3 in an estimation of the optimal k_{off} is in our opinion acceptable for most practical purposes. The total phosphorylation rate also includes the contributions from the untethered reaction paths, which are not considered in Eqs. **1–3**. The agreement will become progressively worse as the contribution of this path increases for higher concentrations and better substrates. For R-3K, both the magnitude and curve shape were predicted relatively well, whereas for R-2K, the curve shape is predicted well but the magnitude is off by a factor of 2. For the optimal substrate, the steady-state phosphorylation rate is independent of docking strength throughout the range tested, and the values agree with the calculated untethered rates. Both the numerical simulations and the analytical solutions suggest some enhancement from the tethering in the fast-k_{off} regime. This implies that some parameters may not be estimated precisely, likely the rate constants of the substrate binding.

Our model is based on the assumption of modularity, meaning that the substrate motif, the linker, and the docking motif can be treated as independent modules. This is clearly a simplification, but it allowed us to assess the contribution of variable elements in the kinase:substrate complex in a general model. Modularity implies structural decoupling between the catalytic domain and the docking interaction. In contrast, allosteric effects of peptide binding typically require direct structural communication between the docking and active sites to affect ATP binding (21, 22) or hinge motions (23). Allosteric effects can typically be ruled out when the docking site is separated from the catalytic domain by a disordered linker. IDRs are common in signaling scaffolds (11) and kinase anchoring proteins (33), which suggests that many docking and catalytic domains will be structurally decoupled. Furthermore, the architecture of kinases, as well as other enzymes like phosphatases (20, 36), are highly modular with similar catalytic domains coupled to diverse protein interaction domains (37). These interactions allow connections to different upstream and downstream partners, ultimately making these systems highly evolvable and adaptable (38). Modularity has been also exploited in biotechnology, bioengineering, and pharmacology (39–41) to successfully rewire signaling processes or modify enzymatic activities. This emergent class of engineered multidomain proteins relies on the easy transfer and exchange (38) of modules, such that design boils down to selecting the right connectors (42). For example, synthetic switches with diverse outputs in response to nonphysiological inputs were made by replacing regulatory domains in *N*-WASP (Wiskott–Aldrich syndrome protein) with heterologous domains and varied linker lengths and substrate-binding affinities (43). In other work, the modular enzyme scaffold has been used to increase metabolic efficiency (44). However, synthetic assemblies do not always work as expected (45), suggesting the need for a theoretical framework to guide the design of enzyme tethers.

These and many other examples (38, 46) support this important phenomenon, giving solid grounds for our mechanistic framework. However, we cannot predict how more integrated systems, where allosteric coupling between modules or different functional units located in a single structure might affect modularity and thus limit the utility of our approach. An example of such a system is Protein Phosphatase 1, where the RVxF binding motif is located in the same domain as the active site (20). In such systems, allostery and tethering act as separate layers of regulation that can operate in parallel. When allosteric effects are present, the passive tethering model presented here can serve as the baseline against which allostery is compared.

Most quantitative studies of enzyme docking interactions considered the catalytic and docking interactions as a single unit. The effect of docking interactions is thus typically to lower K_M, occasionally at the expense of a lowered k_{cat}. However, tethered enzyme reactions are expected to have non-Michaelis–Menten kinetics as illustrated by numerical simulations (*SI Appendix*, Fig. S13). Furthermore, Michaelis–Menten parameters only capture the behavior of a single system but do not predict the effect of other perturbations than concentration. A theoretical model was proposed describing the effect of the energy of the docking interaction on ERK2 phosphorylation, which predicted the existence of an optimal binding strength, although this was not tested experimentally (47). This model ignored the untethered reaction path and is hard to apply in practice, as it is formulated in terms of probability functions and inaccessible rates of intracomplex transitions. The competition between the untethered and tethered rate was described in a recent study using a tethered PKA model system (45). This study uses a modular description similar to ours but observes surprisingly low phosphorylation rates. Like our previous work (5), this study was aimed at single turnover kinetics and did thus not consider product dissociation. The model proposed here incorporates ideas from previous treatments into a single framework expressed in terms that can be measured or estimated. The rate enhancement of docking interactions at affinities below the apex is analogous to the decrease in K_M, and the decrease at high affinities is analogous to decreasing k_{cat} (*SI Appendix*, Fig. S13). The modular description with focus on the docking interaction allows the effect of perturbations to the system to be predicted, which is attractive for design purposes.

Our kinetic framework can be applied to the prediction of the changes associated with mutations in kinases anchoring complexes. Most single nucleotide polymorphisms in docking interactions reduce the affinity. There are many examples from the AKAPs, as follows: The V282M mutation in AKAP18 reduces the interaction with PKA-RIIα ∼9-fold and impairs the cAMP responsive potentiation of L-type Ca^{2+} ion channels (48). The I646V mutation in the dual-specific D-AKAP2 binds ∼3-fold weaker to PKA-RIα, which results in alterations in the subcellular distribution of PKA and cardiac dysfunction (49). The S1570L mutation in AKAP9 reduces the interaction with KCNQ1 and consequently its cAMP-induced phosphorylation causing long-QT cardiac syndrome (50). Furthermore, in an engineered kinase scaffold composed of tandem PDZ domains, kinetic enhancement scaled with PDZ binding affinity (51). In all of these cases, weakening of the interaction reduced phosphorylation rates. Examples of mutations that destabilize docking interactions and lead to up-regulation of phosphorylation are rare. Phosphorylation by cyclin A-Cdk2 was more efficient when the kinase was docked weakly, rather than more strongly, although the kinetics were not characterized in detail (7). In a similar complex, reduction

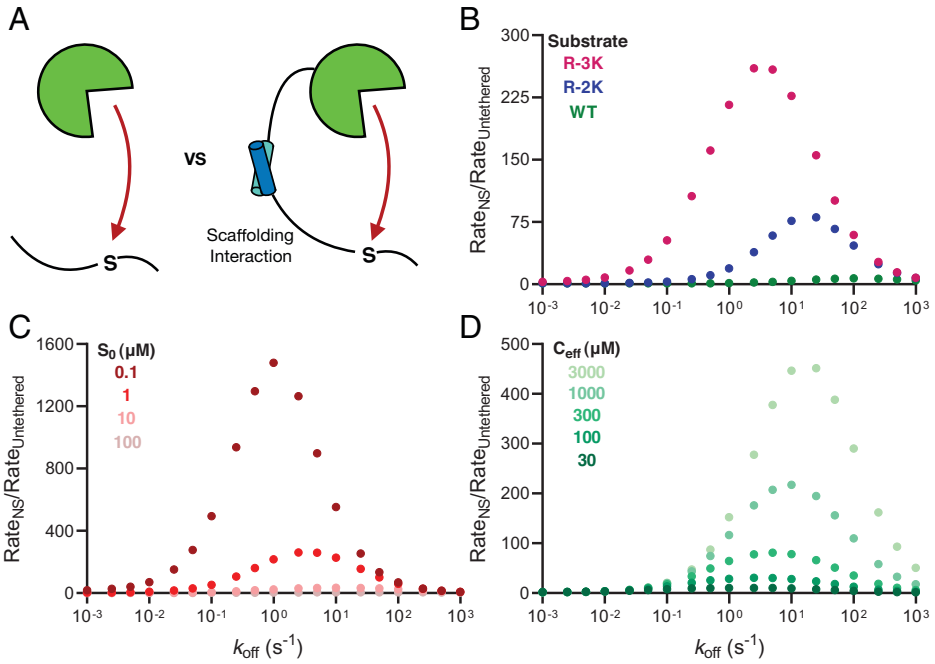

Fig. 5. Kinetic discrimination between tethered and untethered substrates. (*A*) Schematic representation of the untethered vs. reversibly tethered kinase model, where scaffolding interaction results in kinetic rate enhancement. (*B–D*) Comparison of the ratio of a tethered reaction predicted by Eq. **1** to the corresponding untethered reaction predicted by the Michaelis–Menten equation. Unless otherwise mentioned, the substrate is R-3K, [S] = 1 μM and C_{eff} = 388 μM. The largest kinetic boost is observed (*B*) for poor substrates, (*C*) at low substrate concentrations, and (*D*) at high C_{eff}s of the substrate.

occurs due to a reduced catalytic turnover detected as reduced apparent k_{cat} values (15), which has also been seen for MAP kinases (52, 53). We lack the complete kinetic parameters to make proper calculations for these systems, but we can qualitatively explain the effect, as follows: naturally occurring tethered systems might be optimized around intermediate K_D values. Mutations can reduce catalytic efficiency by either increasing or reducing k_{off} and K_D, and thus, both types of mutations may cause pathological phenotypes. Functional predictions for such mutations do not require accurate calculation of rates but rather only to know on which side of the apex a given system is. Therefore, Eqs. **1–3** may be applicable even when some rates are only crudely estimated.

Kinase signaling is rarely optimized for catalytic efficiency but rather for switchability. In terms of tethering interactions, this can be understood as the relative increase in phosphorylation rates in the presence vs. in the absence of a tethering interaction (Fig. 5*A*). Analogously, it can be understood as the ability for a kinase to distinguish the cognate-tethered substrate from a similar noncognate substrate. We thus compared how the kinetic discrimination between an identical tethered and untethered substrate depends on the system parameters (Fig. 5 *B–D*) and formulated the following five general principles for when tethered systems maximize enhancement: 1) enzyme and substrate should interact with intermediate docking strength (typically, K_D in micromolar range), 2) docking interaction should have fast exchange kinetics (high k_{on}/k_{off}) (*SI Appendix*, Fig. S12), 3) the substrate should have low affinity for the enzyme (Fig. 5*B*), 4) the substrate concentrations should be low (Fig. 5*C*), and 5) The connection should be optimized to enforce high C_{eff}s (Fig. 5*D*). As tethered systems with a modular design are not restricted only to kinases (see above), other enzymes can be studied through the same framework, and these rules can be applied as design principles for novel or improved scaffolding interactions. For example, for proximity-based drugs like proteolysis targeting chimeras (PROTACs), it has been recognized that a major obstacle is to generate a design with predictable effects (40). The effectiveness of PROTACs lies in the likelihood to form stable ternary complexes as well as their final concentration after administration (40). In this sense, our approach could be a powerful toolkit to rationally design interactions mediated by scaffolds and optimize drug design/administration as well as predict outcomes of therapeutic treatments.

Data Availability. All study data are included in the article and/or *SI Appendix*.

ACKNOWLEDGMENTS. This work was supported by grants to M.K. from the Young Investigator Program of the Villum Foundation, PROMEMO – Center for Proteins in Memory, a Center of Excellence funded by the Danish National Research Foundation (Grant number DNRF133) and the Novo Nordisk Foundation (NNF20OC0063808). D.E.O. is grateful for support from the Novo Nordisk Foundation (NNF17OC0028806) and the Lundbeck Foundation (R276-2018-671).

Author affiliations: [a]Department of Molecular Biology and Genetics, Aarhus University, DK-8000 Aarhus, Denmark; [b]Interdisciplinary Nanoscience Center (iNANO), Aarhus University, DK-8000 Aarhus, Denmark; [c]The Danish Research Institute for Translational Neuroscience (DANDRITE), Nordic EMBL Partnership for Molecular Medicine, DK-8000 Aarhus, Denmark; and [d]Center for Proteins in Memory - PROMEMO, Danish National Research Foundation, DK-8000 Aarhus, Denmark

1. C. J. Miller, B. E. Turk, Homing in: Mechanisms of substrate targeting by protein kinases. *Trends Biochem. Sci.* **43**, 380–394 (2018).
2. W. Wong, J. D. Scott, AKAP signalling complexes: Focal points in space and time. *Nat. Rev. Mol. Cell Biol.* **5**, 959–970 (2004).
3. J. D. Scott, T. Pawson, Cell signaling in space and time: Where proteins come together and when they're apart. *Science* **326**, 1220–1224 (2009).
4. M. C. Good, J. G. Zalatan, W. A. Lim, Scaffold proteins: Hubs for controlling the flow of cellular information. *Science* **332**, 680–686 (2011).
5. M. Dyla, M. Kjaergaard, Intrinsically disordered linkers control tethered kinases via effective concentration. *Proc. Natl. Acad. Sci. U.S.A.* **117**, 21413–21419 (2020).
6. B. A. Schulman, D. L. Lindstrom, E. Harlow, Substrate recruitment to cyclin-dependent kinase 2 by a multipurpose docking site on cyclin A. *Proc. Natl. Acad. Sci. U.S.A.* **95**, 10453–10458 (1998).
7. P. Guida, L. Zhu, DP1 phosphorylation in multimeric complexes: Weaker interaction with cyclin A through the E2F1 cyclin A binding domain leads to more efficient phosphorylation than stronger interaction through the p107 cyclin A binding domain. *Biochem. Biophys. Res. Commun.* **258**, 596–604 (1999).
8. D. Y. Takeda, J. A. Wohlschlegel, A. Dutta, A bipartite substrate recognition motif for cyclin-dependent kinases. *J. Biol. Chem.* **276**, 1993–1997 (2001).
9. J. Kragelj *et al.*, Structure and dynamics of the MKK7-JNK signaling complex. *Proc. Natl. Acad. Sci. U.S.A.* **112**, 3409–3414 (2015).

10. W. Peti, R. Page, Molecular basis of MAP kinase regulation. *Protein Sci.* **22**, 1698–1710 (2013).
11. M. S. Cortese, V. N. Uversky, A. K. Dunker, Intrinsic disorder in scaffold proteins: Getting more from less. *Prog. Biophys. Mol. Biol.* **98**, 85–106 (2008).
12. C. S. Sørensen, M. Kjaergaard, Effective concentrations enforced by intrinsically disordered linkers are governed by polymer physics. *Proc. Natl. Acad. Sci. U.S.A.* **116**, 23124–23131 (2019).
13. C. Hundsrucker *et al.*, High-affinity AKAP7δ-protein kinase A interaction yields novel protein kinase A-anchoring disruptor peptides. *Biochem. J.* **396**, 297–306 (2006).
14. N. E. Davey *et al.*, Attributes of short linear motifs. *Mol. Biosyst.* **8**, 268–281 (2012).
15. L. M. Stevenson-Lindert, P. Fowler, J. Lew, Substrate specificity of CDK2-cyclin A. What is optimal? *J. Biol. Chem.* **278**, 50956–50960 (2003).
16. H. Li, L. Zhang, A. Rao, S. C. Harrison, P. G. Hogan, Structure of calcineurin in complex with PVIVIT peptide: Portrait of a low-affinity signalling interaction. *J. Mol. Biol.* **369**, 1296–1306 (2007).
17. P. H. Sabatier, Hydrogénations et déshydrogénations par catalyse. *Ber. Dtsch. Chem. Ges.* **44**, 1984–2001 (1911).
18. J. Kari *et al.*, Sabatier principle for interfacial (heterogeneous) enzyme catalysis. *ACS Catal.* **8**, 11966–11972 (2018).
19. R. M. Gordley, L. J. Bugaj, W. A. Lim, Modular engineering of cellular signaling proteins and networks. *Curr. Opin. Struct. Biol.* **39**, 106–114 (2016).
20. W. Peti, A. C. Nairn, R. Page, Structural basis for protein phosphatase 1 regulation and specificity. *FEBS J.* **280**, 596–611 (2013).
21. Y.-S. Heo *et al.*, Structural basis for the selective inhibition of JNK1 by the scaffolding protein JIP1 and SP600125. *EMBO J.* **23**, 2185–2195 (2004).
22. Y. Tokunaga, K. Takeuchi, H. Takahashi, I. Shimada, Allosteric enhancement of MAP kinase p38α's activity and substrate selectivity by docking interactions. *Nat. Struct. Mol. Biol.* **21**, 704–711 (2014).
23. R. P. Bhattacharyya *et al.*, The Ste5 scaffold allosterically modulates signaling output of the yeast mating pathway. *Science* **311**, 822–826 (2006).
24. S. Lee *et al.*, Examining docking interactions on ERK2 with modular peptide substrates. *Biochemistry* **50**, 9500–9510 (2011).
25. B. Schuler, A. Soranno, H. Hofmann, D. Nettels, Single-molecule FRET spectroscopy and the polymer physics of unfolded and intrinsically disordered proteins. *Annu. Rev. Biophys.* **45**, 207–231 (2016).
26. C. Kalthoff, A novel strategy for the purification of recombinantly expressed unstructured protein domains. *J. Chromatogr. B Analyt. Technol. Biomed. Life Sci.* **786**, 247–254 (2003).
27. K. A. Johnson, Z. B. Simpson, T. Blom, Global kinetic explorer: A new computer program for dynamic simulation and fitting of kinetic data. *Anal. Biochem.* **387**, 20–29 (2009).
28. B. D. Grant, J. A. Adams, Pre-steady-state kinetic analysis of cAMP-dependent protein kinase using rapid quench flow techniques. *Biochemistry* **35**, 2022–2029 (1996).
29. M. Kjaergaard, Estimation of effective concentrations enforced by complex linker architectures from conformational ensembles. *Biochemistry* **61**, 171–182 (2022).
30. B. E. Kemp, D. J. Graves, E. Benjamini, E. G. Krebs, Role of multiple basic residues in determining the substrate specificity of cyclic AMP-dependent protein kinase. *J. Biol. Chem.* **252**, 4888–4894 (1977).
31. M. N. Gnanapragasam *et al.*, p66α-MBD2 coiled-coil interaction and recruitment of Mi-2 are critical for globin gene silencing by the MBD2-NuRD complex. *Proc. Natl. Acad. Sci. U.S.A.* **108**, 7487–7492 (2011).
32. G. Schreiber, G. Haran, H.-X. Zhou, Fundamental aspects of protein-protein association kinetics. *Chem. Rev.* **109**, 839–860 (2009).
33. M. Dyla, M. Kjaergaard, "Intrinsic disorder in protein kinase A anchoring proteins signaling complexes" in *Dancing Protein Clouds: Intrinsically Disordered Proteins in the Norm and Pathology, Part C*, V. N. Uversky, Ed. (*Progress in Molecular Biology and Translational Science*, Academic Press, 2021), **vol. 183**, pp. 271–294.
34. J. Dogan, J. Jonasson, E. Andersson, P. Jemth, Binding rate constants reveal distinct features of disordered protein domains. *Biochemistry* **54**, 4741–4750 (2015).
35. S. Gianni, J. Dogan, P. Jemth, Coupled binding and folding of intrinsically disordered proteins: What can we learn from kinetics? *Curr. Opin. Struct. Biol.* **36**, 18–24 (2016).
36. J. Goyette *et al.*, Biophysical assay for tethered signaling reactions reveals tether-controlled activity for the phosphatase SHP-1. *Sci. Adv.* **3**, e1601692 (2017).
37. B. J. Mayer, The discovery of modular binding domains: Building blocks of cell signalling. *Nat. Rev. Mol. Cell Biol.* **16**, 691–698 (2015).
38. R. P. Bhattacharyya, A. Reményi, B. J. Yeh, W. A. Lim, Domains, motifs, and scaffolds: The role of modular interactions in the evolution and wiring of cell signaling circuits. *Annu. Rev. Biochem.* **75**, 655–680 (2006).
39. S. Gad, S. Ayakar, Protein scaffolds: A tool for multi-enzyme assembly. *Biotechnol. Rep. (Amst.)* **32**, e00670 (2021).
40. M. Maneiro *et al.*, PROTACs, molecular glues and bifunctionals from bench to bedside: Unlocking the clinical potential of catalytic drugs. *Prog. Med. Chem.* **60**, 67–190 (2021).
41. E. M. Hobert, A. E. Doerner, A. S. Walker, A. Schepartz, Effective molarity *redux*: Proximity as a guiding force in chemistry and biology. *Isr. J. Chem.* **53**, 567–576 (2013).
42. A. Gräwe, V. Stein, Linker engineering in the context of synthetic protein switches and sensors. *Trends Biotechnol.* **39**, 731–744 (2021).
43. J. E. Dueber, B. J. Yeh, K. Chak, W. A. Lim, Reprogramming control of an allosteric signaling switch through modular recombination. *Science* **301**, 1904–1908 (2003).
44. J. E. Dueber *et al.*, Synthetic protein scaffolds provide modular control over metabolic flux. *Nat. Biotechnol.* **27**, 753–759 (2009).
45. E. B. Speltz, J. G. Zalatan, The relationship between effective molarity and affinity governs rate enhancements in tethered kinase-substrate reactions. *Biochemistry* **59**, 2182–2193 (2020).
46. A. H. C. Horn, H. Sticht, Synthetic protein scaffolds based on peptide motifs and cognate adaptor domains for improving metabolic productivity. *Front. Bioeng. Biotechnol.* **3**, 191 (2015).
47. M. M. Misiura, A. B. Kolomeisky, Theoretical investigation of the mechanisms of ERK2 enzymatic catalysis. *J. Phys. Chem. B* **120**, 10508–10514 (2016).
48. F. D. Smith *et al.*, Single nucleotide polymorphisms alter kinase anchoring and the subcellular targeting of A-kinase anchoring proteins. *Proc. Natl. Acad. Sci. U.S.A.* **115**, E11465–E11474 (2018).
49. S. Kammerer *et al.*, Amino acid variant in the kinase binding domain of dual-specific A kinase-anchoring protein 2: A disease susceptibility polymorphism. *Proc. Natl. Acad. Sci. U.S.A.* **100**, 4066–4071 (2003).
50. L. Chen *et al.*, Mutation of an A-kinase-anchoring protein causes long-QT syndrome. *Proc. Natl. Acad. Sci. U.S.A.* **104**, 20990–20995 (2007).
51. J. Ryu, S.-H. Park, Simple synthetic protein scaffolds can create adjustable artificial MAPK circuits in yeast and mammalian cells. *Sci. Signal.* **8**, ra66 (2015).
52. N. Fernandes, D. E. Bailey, D. L. Vanvranken, N. L. Allbritton, Use of docking peptides to design modular substrates with high efficiency for mitogen-activated protein kinase extracellular signal-regulated kinase. *ACS Chem. Biol.* **2**, 665–673 (2007).
53. N. Fernandes, N. L. Allbritton, Effect of the DEF motif on phosphorylation of peptide substrates by ERK. *Biochem. Biophys. Res. Commun.* **387**, 414–418 (2009).